

Development of a Novel Free Molecule Rocket Plume Model

Michael Woronowicz

*Swales Aerospace
5050 Powder Mill Road
Beltsville, Maryland 20705, USA*

Abstract. This paper describes development of a set of analytic point source transient free molecule equations generated to model behavior ranging from molecular effusion to rocket plumes. A brief review of model performance for step function mass expulsion will be followed by presentation of physical extensions to include the effects of an ellipsoidal molecular distribution to account for certain types of thermal nonequilibrium, and response to sources described by pulse as well as step function behavior.

INTRODUCTION

Analysis and simulation of gases expanding from sources into vacuum, or the effects plumes from these sources create when they interact with solid surfaces, present a considerable challenge to the scientific and engineering communities. The main difficulty lies in accurately describing a flowfield that passes from continuum flow at the nozzle exit, through the transition regime, to free molecule behavior within a relatively short distance downstream.

For rocket engines and chemical thrusters, high velocity levels and relatively high Mach numbers typically characterize flow at the nozzle exit. Within the plume's core, even in regions where significant intermolecular collision rates occur, relative velocity levels are low and little thermal scattering occurs normal to the mainly radial streamlines. Under certain circumstances, such observations lead one to consider describing the expansion using free molecule theory.

Development of such a model began a few years ago to provide insights for DSMC simulations of Shuttle/Mir docking scenarios.⁽¹⁾ This paper briefly reviews steady model performance for a variety of cases, followed by development of physical extensions for an ellipsoidal molecular distribution and response to sources described by pulse as well as step function behavior.

MODEL FORMULATION

A transient solution of the collisionless Boltzmann equation was developed to describe the molecular distribution $f(x,t)$ for flow from a point source step function Q_1 , where (1-3)

$$\frac{\partial f}{\partial t} + \mathbf{v} \cdot \frac{\partial f}{\partial \mathbf{x}} = Q_1; \quad Q_1 = \frac{2\beta^4}{A_1\pi} \delta(\mathbf{x}) \dot{m}(t) |\mathbf{v} \cdot \hat{\mathbf{n}}| \exp\left(-\beta^2(\mathbf{v} - \mathbf{u}_e)^2\right). \quad (1)$$

Report Documentation Page

Report Date 09JUL2000	Report Type N/A	Dates Covered (from... to) -
Title and Subtitle Development of a Novel Free Molecule Rocket Plume Model		Contract Number
		Grant Number
		Program Element Number
Author(s)		Project Number
		Task Number
		Work Unit Number
Performing Organization Name(s) and Address(es) Swales Aerospace 5050 Powder Mill Road Beltsville, Maryland 20705		Performing Organization Report Number
Sponsoring/Monitoring Agency Name(s) and Address(es) AOARD Unit 45002 APO AP 96337-5002		Sponsor/Monitor's Acronym(s)
		Sponsor/Monitor's Report Number(s)
Distribution/Availability Statement Approved for public release, distribution unlimited		
Supplementary Notes Papers from Rarefied Gas Dynamics (RGD) 22nd International Symposium held in Sydney, Australia on 9-14 July 2000. See also ADM001341 for whole conference on cd-rom., The original document contains color images.		
Abstract		
Subject Terms		
Report Classification unclassified		Classification of this page unclassified
Classification of Abstract unclassified		Limitation of Abstract UU
Number of Pages 8		

In Eq. (1), Q_1 represents source flow with a Lambertian thermal distribution superimposed on a convective exit velocity u_e at constant rate \dot{m} . The $\mathbf{v} \cdot \hat{\mathbf{n}}$ factor emphasizes the directional constraint imposed by the rocket nozzle. Parameter $\beta \equiv 1/\sqrt{2RT}$, and A_1 is a normalization factor (5) defined as:

$$A_1 \equiv e^{-s^2 \cos^2 \phi_e} + \sqrt{\pi} s \cos \phi_e (1 + \operatorname{erf}(s \cos \phi_e)). \quad (2)$$

Fig. 1 describes the general relationship between important geometric elements in this model.

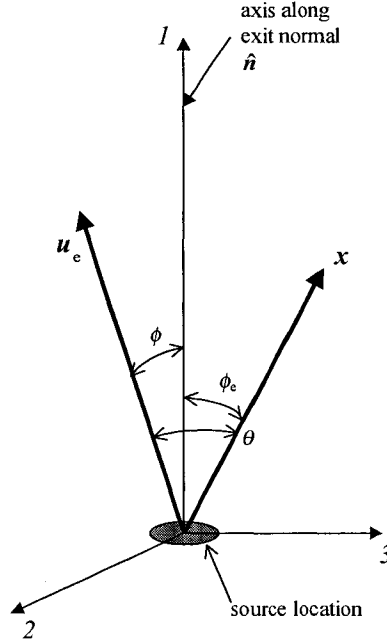


FIGURE 1: Schematic representation of various quantities and angles used in analytic model.

Speed ratio $s \equiv \beta u_e$, and $\hat{\mathbf{n}}$ represents the nozzle exit plane. Generally, u_e may not be aligned with $\hat{\mathbf{n}}$. Angle ϕ_e lies between u_e and $\hat{\mathbf{n}}$, ϕ is measured between variable position \mathbf{x} (with velocity \mathbf{v}) and $\hat{\mathbf{n}}$, and angle θ is measured between u_e and \mathbf{x} . For axisymmetric conditions, $\phi_e = 0$ and $\phi = \theta$.

The particular solution of Eq. (1) is found using the approach outlined by Bird (6) and Narasimha (7). The steady-state density field generated in response to a step function in mass flow rate \dot{m} , with constant properties across the nozzle exit, is given by (1)

$$\rho(\mathbf{x}, t) = \frac{\beta \dot{m} \cos \phi}{A_1 \pi r^2} e^{w^2 - s^2} \left\{ (\alpha + w) e^{-z^2} + \left(\frac{1}{2} + w^2 \right) \sqrt{\pi} \operatorname{erfc} z \right\}, \quad (3)$$

where $z \equiv \alpha - w$, $\alpha \equiv \beta r/t$, and $w \equiv s \cos \theta$. Solving for successive velocity moments, one obtains expressions for mass flux $\dot{\Phi}$, normal momentum flux ("pressure") p_\perp , and translational energy flux \dot{q}_{TR} :(1)

$$\dot{\Phi}(\mathbf{x}, t) = \frac{\dot{m} \cos \phi}{A_1 \pi r^2} \frac{\mathbf{x}}{r} e^{w^2 - s^2} \left\{ \left(\alpha^2 + \alpha w + w^2 + 1 \right) e^{-z^2} + \left(\frac{3}{2} + w^2 \right) \sqrt{\pi} w \operatorname{erfc} z \right\}, \quad (4)$$

$$p_{\perp}(x, t) = \frac{\dot{m} \cos \phi}{\beta A_1 \pi r^2} e^{w^2 - s^2} \left\{ \left(\alpha^3 + \alpha^2 w + \alpha w^2 + w^3 + \frac{5}{2} w + \frac{3}{2} \alpha \right) e^{-z^2} + \left(\frac{3}{4} + 3 w^2 + w^4 \right) \sqrt{\pi} \operatorname{erfc} z \right\}, \quad (5)$$

$$\dot{q}_{\text{TR}}(x, t) = \frac{\dot{m} \cos \phi}{2 \beta^2 A_1 \pi r^2} \frac{x}{r} e^{w^2 - s^2} \left\{ \left(\alpha^4 + \alpha^3 w + \alpha^2 w^2 + \alpha w^3 + w^4 + 2 \alpha^2 + \frac{7}{2} \alpha w + \frac{9}{2} w^2 + 2 \right) e^{-z^2} + \left(\frac{15}{4} + 5 w^2 + w^4 \right) \sqrt{\pi} w \operatorname{erfc} z \right\}. \quad (6)$$

In addition, Eqns. (3) – (5) may be combined to obtain expressions for velocity v , translational temperature T_{TR} , and internal energy flux \dot{q}_{INT} for polyatomic molecules with specific heat ratio γ :

$$v(x) = \frac{\Phi(x)}{\rho(x)}; \quad T_{\text{TR}}(x) = \frac{1}{3R} \left\{ \frac{p_{\perp}(x)}{\rho(x)} - (v(x))^2 \right\}; \quad \dot{q}_{\text{INT}}(x) = \left(\frac{5-3\gamma}{\gamma-1} \right) \frac{\Phi(x)}{4\beta^2}. \quad (7)$$

The single source solution is only valid where $x \cdot \hat{n} > 0$ due to the velocity constraint in Eq. (1). It also assumes constant, averaged properties describe the gas issuing from the nozzle. A more realistic analysis would incorporate locally varying conditions across the exit. This data would be used to create a network of point sources to describe the expansion downstream. An even more sophisticated approach would involve superposition of a source network located on a “freezing surface” downstream from the nozzle, whose properties have been computed using a coupled CFD/DSMC approach.(1)

CASE REVIEWS

This model was initially applied to a study concerning Shuttle/Mir interactions. Results were used to adapt DSMC grids for better computational efficiency and to verify collisionless DSMC results.(1) The following sections describe highlights from other studies using the analytic technique.

Nitrogen Thruster

In a previously unpublished study conducted at NASA Langley Research Center, analytic model results were compared to three-dimensional direct simulation Monte Carlo computations (NASA-LaRC’s DSMC3 code) for steady flow from a small cold nitrogen gas thruster. Starting conditions consisted of properties averaged across the thruster’s exit plane ($n = 4 \times 10^{20} / \text{m}^3$, $V = 730 \text{ m/s}$, $T = 40 \text{ K}$). Analytic results utilized a network of 320 sources superimposed across the nozzle exit area. DSMC calculations were performed in collisionless and collisional modes to assess this effect on the results.

Dimensionless logarithmic density contour maps are presented in Fig. 2 for over four orders of magnitude. The uppermost contour map features the analytic model solution, and at center are virtually identical collisionless DSMC results. The lowest contour map depicts full DSMC results, showing shorter, slightly broader contours than the collisionless cases as a direct manifestation of collisional scattering. Overall, analytic model results still produce quite reasonable agreement with the full DSMC simulation. It became evident *post hoc* that virtually the entire simulation had been performed within the Bird continuum breakdown surface signifying the onset of transitional flow deviations from continuum conditions.(1) Since collisional effects usually dominate such flows, this study provided particularly harsh conditions for testing the free molecule analytic technique.

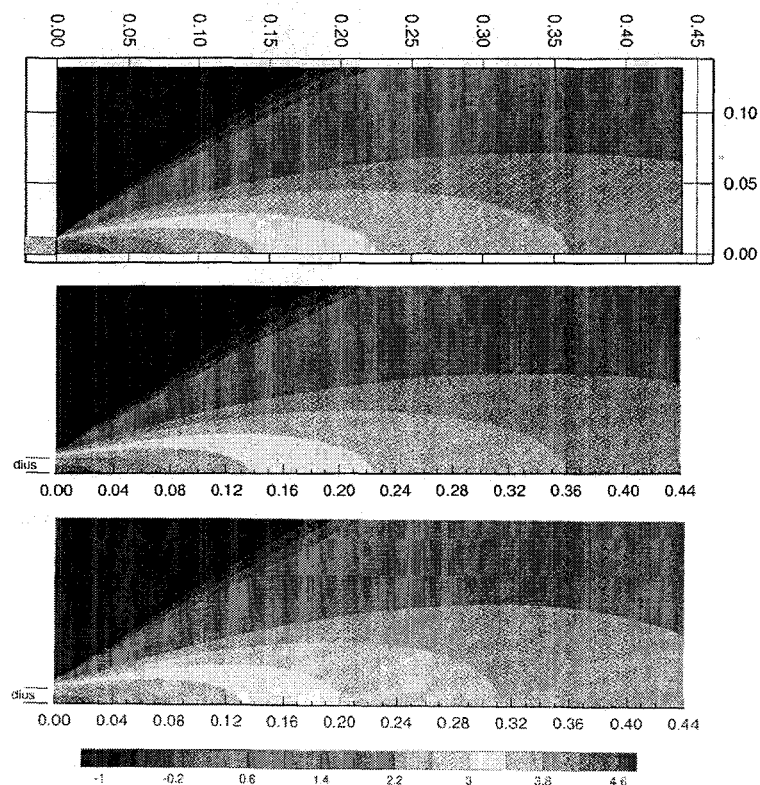


FIGURE 2: Comparison of steady-state density contours for a small N_2 axisymmetric thruster. Physical scale in m, logarithmic dimensionless density scale. Top: analytic results; middle: collisionless DSMC; bottom: full DSMC (with intermolecular collisions). DSMC calculations performed by Dr. Richard Wilmoth, NASA-LaRC.

Sonic Orifice

Although comparisons made for the previous case were very favorable, solutions were propagated from a flat profile of macroscopic variables across the nozzle exit. The presence of an annular shear layer containing thermodynamic properties differing from the core would increase the influence of collisional scattering, particularly in terms of self-scattered return flux ahead of the nozzle's exit plane. In another previously unpublished study, comparisons were made between analytic and full DSMC3 results for steady nitrogen gas flow through a sharp-edged sonic orifice in high vacuum. Both techniques used the same network of conditions mapped on a starting surface created from a previously generated CFD expansion solution.

Figure 3 shows excellent agreement between the two approaches for density contours over one order of magnitude. As in the previous case, DSMC results were considered somewhat in error at high angles off the centerline due to cell resolution limitations. Similar levels of agreement between the two techniques were found for comparisons of mass flux, normal momentum flux, and velocity.

Bipropellant Thruster

A Messerschmitt-Bolkow-Blohm (MBB) 10 N monomethyl hydrazine/nitrogen tetroxide (MMH/ N_2O_4) bipropellant thruster was modeled using a single point source (2) to make comparisons with a relatively comprehensive set of previously published experimental data.(8-11) Based on a combination of published and derived information, the necessary average exit conditions were obtained ($s = 3.11$, $MW = 26$ amu, $\dot{m} = 3.5$ g/s, specific heat ratio $\gamma = 1.322$, and velocity $u_e = 3056$ m/s).(2)

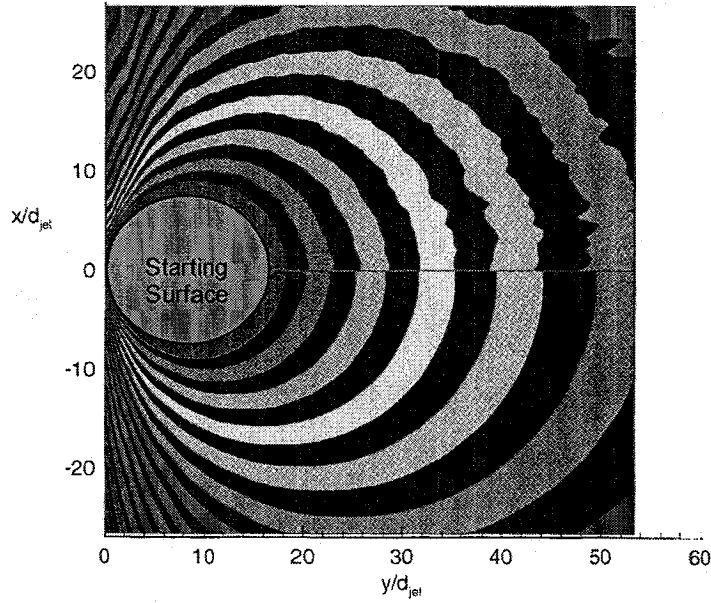


FIGURE 3: Steady-state density contours for N_2 flow through a sonic orifice. Logarithmic dimensionless density scale. Top—DSMC; bottom—analytic model. Calculations performed by Dr. Richard Wilmoth, NASA-LaRC.

Model results were compared to distributions for force and contaminant mass fluence (MMH-nitrate).(2) For relatively high w , model force and mass flux angular distribution ratios simplify to

$$\frac{F(r, \theta)}{F(r, 0)} = \frac{p_{\perp}(r, \theta)}{p_{\perp}(r, 0)} \equiv \cos \theta e^{w^2 - s^2} \left[\frac{\frac{3}{4} + 3w^2 + w^4}{\frac{3}{4} + 3s^2 + s^4} \right]; \quad \frac{\dot{\Phi}(r, \theta)}{\dot{\Phi}(r, 0)} \equiv \cos^2 \theta e^{w^2 - s^2} \left[\frac{3 + 2w^2}{3 + 2s^2} \right]. \quad (8)$$

It is evident these ratios are not identical, with \dot{m} exhibiting more angular sensitivity than p_{\perp} . This result differs from the Simons model, where one usually assumes all such distributions are described by $f(\theta) \propto \cos^n \theta$.(12) For further comparison, normalized angular distributions were also plotted for the Simons model with $n = 8.65$, a typical small bipropellant thruster parameter.(12) In Fig. 4, the analytic model force distribution provides a much more precise fit to the data than does the Simons model.

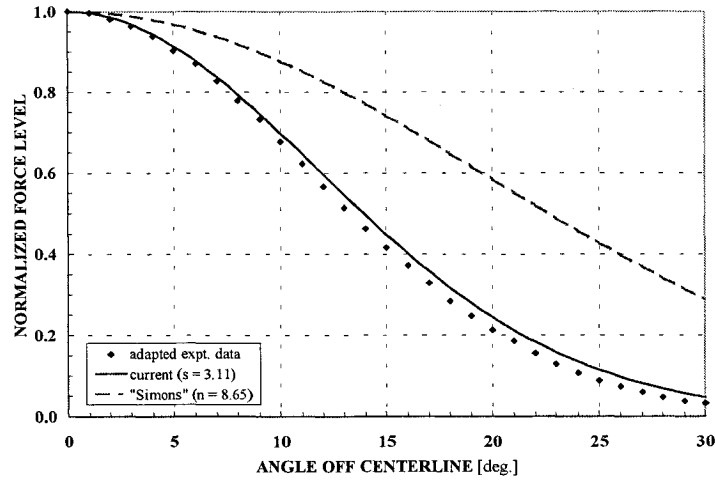


FIGURE 4: Normalized experimental and theoretical force distributions for MBB 10 N thruster.

Fluence comparisons were complicated by multiphase effects, which noticeably affected experimental data within 5° of the centerline.(2) A related investigation into thruster contamination indicated MMH-nitrate deposition may be limited by transport of N_2O_4 , with the contaminant being formed on target surfaces rather than within the thruster.(2,13) Due to a natural species separation effect in free molecule flow, it was decided to replace s by $s_{N_2O_4}$ ($= 5.85$) in the mass flux ratio.

Figure 5 presents normalized MMH-nitrate fluence distributions deposited during a 40 ms thruster pulse. The data was arbitrarily increased by $1.6\times$ to account for significant droplet influence within 5° off centerline. The shifted distribution becomes closely matched for $\theta \geq 5^\circ$ by model results for $s_{N_2O_4}$. In addition, theoretical deposition levels based on experimentally reported unburned propellant fraction were very close to measurements (numerically identical, not accounting for the $1.6\times$ shift).(2) The experimental data's angular variation precluded similar matching with the Simons model for any amount of shifting with $n = 8.65$.

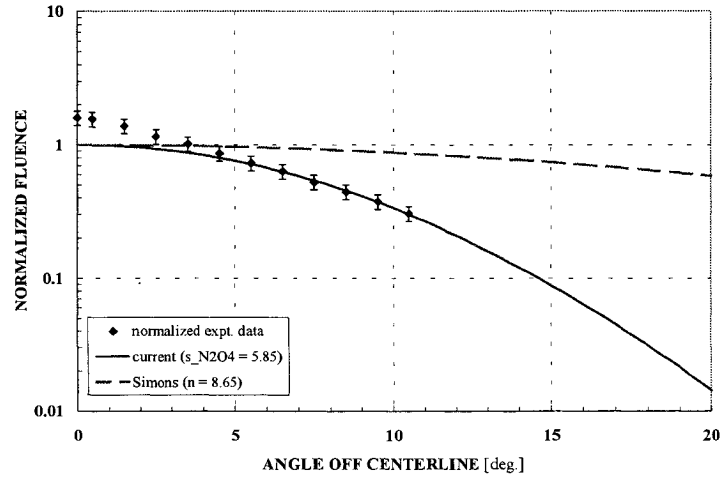


FIGURE 5: Normalized experimental and theoretical MMH-nitrate fluence distributions for MMB 10 N thruster.

ELLIPSOIDAL DISTRIBUTION

The ellipsoidal thermal distribution assumes one may describe departures from thermal equilibrium by assigning an effective one-dimensional temperature to each direction in space.(4) It becomes convenient to modify the constant source term from Eq. (1) in the following manner:

$$\tilde{Q}_1 = \frac{2\beta_1^2\beta_2\beta_3}{A_1\pi} \delta(\mathbf{x}) \dot{m}(t) |\mathbf{v} \cdot \hat{\mathbf{n}}| e^{-(\tilde{\alpha} - \tilde{s})^2}, \text{ where } \tilde{A}_1 \equiv e^{-s_1^2 \cos^2 \phi_e} + \sqrt{\pi} s_1 \cos \phi_e (1 + \text{erf}(s_1 \cos \phi_e)). \quad (9)$$

Referring to Fig. 1, subscript 1 denotes the direction along $\hat{\mathbf{n}}$, with 2 & 3 normal to 1 . Thermal parameter β_i is affected by the definition of three one-dimensional temperatures to replace T . Tildes in Eq. (9) denote component nondimensionalization of variables by β_i . This development in turn affects the description of wave velocity $\tilde{\alpha} \equiv (\beta \mathbf{v})_i = (\beta x)_i / t$, and it becomes convenient to redefine speed ratio s as a vector. In addition, normalization parameter \tilde{A}_1 becomes modified, and the definition for angle θ becomes distorted through nondimensionalization by unlike components of β_i . The latter no longer represents the physical angle between \mathbf{v} and \mathbf{u}_e but rather:

$$\cos \theta \equiv \frac{\tilde{\alpha} \cdot \tilde{s}}{|\tilde{\alpha}| |\tilde{s}|}. \quad (10)$$

Straightforward derivation reveals velocity moments corresponding to the solution of the Boltzmann equation due to source term \tilde{Q}_1 . In the following equations, $z' \equiv \alpha' - w'$, $\alpha' \equiv |\tilde{\alpha}|$, and $w' \equiv |\tilde{s}| \cos \theta$. When all three one-dimensional temperatures are equivalent, Eqns. (11)-(14) reduce to Eqns. (3)-(6).

$$\rho(x, t) = \frac{\dot{m} \beta_1^2 \beta_2 \beta_3}{\tilde{A}_1 \pi} \frac{r \cos \phi}{\tilde{r}^3} e^{-\tilde{s}^2 \sin^2 \theta} \left\{ (\alpha' + w') e^{-z'^2} + \left(\frac{1}{2} + w'^2 \right) \sqrt{\pi} \operatorname{erfc} z' \right\}, \quad (11)$$

$$\Phi(x, t) = \frac{\dot{m} \beta_1^2 \beta_2 \beta_3}{\tilde{A}_1 \pi} \frac{x r \cos \phi}{\tilde{r}^4} e^{-\tilde{s}^2 \sin^2 \theta} \left\{ (\alpha'^2 + \alpha' w' + w'^2 + 1) e^{-z'^2} + \left(\frac{3}{2} + w'^2 \right) \sqrt{\pi} w' \operatorname{erfc} z' \right\}, \quad (12)$$

$$p_{\perp}(x, t) = \frac{\dot{m} \beta_1^2 \beta_2 \beta_3}{\tilde{A}_1 \pi} \frac{r^3 \cos \phi}{\tilde{r}^5} e^{-\tilde{s}^2 \sin^2 \theta} \left\{ \left(\alpha'^3 + \alpha'^2 w' + \alpha' w'^2 + w'^3 + \frac{5}{2} w' + \frac{3}{2} \alpha' \right) e^{-z'^2} + \left(\frac{3}{4} + 3 w'^2 + w'^4 \right) \sqrt{\pi} \operatorname{erfc} z' \right\}, \quad (13)$$

$$\dot{q}_{\text{TR}}(x, t) = \frac{\dot{m} \beta_1^2 \beta_2 \beta_3}{2 \tilde{A}_1 \pi} \frac{x r^3 \cos \phi}{\tilde{r}^6} e^{-\tilde{s}^2 \sin^2 \theta} \left\{ \left(\alpha'^4 + \alpha'^3 w' + \alpha'^2 w'^2 + \alpha' w'^3 + w'^4 + 2 \alpha'^2 + \frac{7}{2} \alpha' w' + \frac{9}{2} w'^2 + 2 \right) e^{-z'^2} + \left(\frac{15}{4} + 5 w'^2 + w'^4 \right) \sqrt{\pi} w' \operatorname{erfc} z' \right\}. \quad (14)$$

When the constant mass rate \dot{m} is replaced by a Delta function $m \delta(t)$, a simpler set of velocity moments is produced. Convolution of these equations at constant strength reproduce Eqns. (13)-(16), and they reduce to the thermal equilibrium case in an analogous manner when $T_1 = T_2 = T_3 = T$.

$$\rho(x, t) = \frac{2 m \beta_1^2 \beta_2 \beta_3}{\tilde{A}_1 \pi} \frac{r \cos \phi}{t^4} e^{-(\tilde{\alpha} - \tilde{s})^2}; \quad \Phi(x, t) = \frac{\rho x}{t}; \quad p_{\perp}(x, t) = \frac{\rho r^2}{t^2}; \quad \dot{q}_{\text{TR}}(x, t) = \frac{\rho r^2 x}{2 t^3}. \quad (15)$$

CONCLUDING REMARKS

The plume model described herein appears to exhibit a good measure of promise for advancing the ability to predict neutral gaseous plume expansions under rarefied conditions. In the near future, it is intended to combine this model with the Bhatnagar-Gross-Krook (BGK) technique (14) in order to develop a return flux capability for analyzing contamination effects on satellites due to self-scattering and ambient scattering of rocket plume products.

ACKNOWLEDGMENTS

The author gratefully acknowledges support from NASA Contract NAS5-32650, and from Dr. Richard G. Wilmoth, NASA-LaRC, for use of his DSMC comparison results.

REFERENCES

1. Woronowicz, M. S., and Rault, D. F. G., "On Plume Flowfield Analysis and Simulation Techniques," *AIAA Paper No. 94-2048*, 6th AIAA/ASME Joint Thermophysics and Heat Transfer Conference, Colorado Springs, CO, June 1994.
2. Woronowicz, M. S., "Experimental Validation of a Simple Bipropellant Thruster Plume Model," *AIAA Paper No. 2000-0598*, 38th AIAA Aerospace Sciences Meeting, Reno, NV, January 2000.
3. Woronowicz, M. S., "Initial Molecular Flow Observations On Bipolar Planetary Nebulae Gaskinetics," *AIAA Paper No. 2000-0599*, 38th AIAA Aerospace Sciences Meeting, Reno, NV, January 2000.
4. Willis, D. R., and Hamel, B. B., "Non-Equilibrium Effects in Spherical Expansions of Polyatomic Gases and Gas Mixtures," *Rarefied Gas Dynamics*, (Proceedings of the 5th International Symposium), ed. Brundin, C. L., 1, Academic Press, 1967, pp. 837-861.
5. Cercignani, C., *The Boltzmann Equation and Its Applications*, Applied Mathematical Series 67, Springer Verlag, 1988, ch. 3, pp. 134-137.
6. Bird, G. A., *Molecular Gas Dynamics and the Direct Simulation of Gas Flows*, Oxford, Clarendon Press, 1994, ch. 4, pp. 77-88.
7. Narasimha, R., "Collisionless expansion of gases into vacuum," *Journal of Fluid Mechanics*, 12, No. 1, 1962, pp. 294-308.
8. Trinks, H., "Experimental Exhaust Plume Analysis with MBB 10 N Thruster," *AIAA Paper No. 83-1259*, 19th AIAA/SAE/ASME Joint Propulsion Conference, Seattle, WA, June 1983.
9. Trinks, H., and Hoffman, R. J., "Experimental Investigation of Bipropellant Exhaust Plume Flowfield, Heating and Contamination..." *AIAA Paper No. 83-1447*, 18th AIAA Thermophysics Conference, Montreal, Quebec, Canada, June 1983.
10. Hoffman, R. J., et al., "The CONTAM 3.2 Plume Flowfield Analysis and Contamination Prediction Computer Program: Analysis Model and Experimental Verification," *AIAA Paper No. 85-0928*, 20th AIAA Thermophysics Conference, Williamsburg, VA, June 1985.
11. Trinks, H., and Hoffman, R. J., "Standard Experimental Exhaust Plume Analysis Procedure in Connection with CONTAM Computer Model Predictions" *AIAA Paper No. 85-1390*, 21st AIAA/SAE/ASME/ASEE Joint Propulsion Conference, Monterey, CA, July 1985.
12. *Shuttle/Payload Contamination Evaluation Program User's Manual*, Version 2, and NASA JSC Document No. MCR-81-509, Martin Marietta Corp., Denver Aerospace.
13. Woronowicz, M. S., "Alternative Description of MMH-Nitrate Formation Due to Bipropellant Thrusters," *AIAA Paper No. 2000-0604*, 38th AIAA Aerospace Sciences Meeting, Reno, NV, January 2000.
14. Bhatnagar, P. L., et al., "A Model for Collision Processes in Gases..." *Physical Review*, 94, No. 3, May 1954, pp. 511-25.